



ELSEVIER

Available online at www.sciencedirect.com

SCIENCE @ DIRECT®

Journal of Magnetic Resonance xxx (2004) xxx–xxx

JMR

Journal of
Magnetic Resonance

www.elsevier.com/locate/jmr

Magnetic material arrangement in oriented termites: a magnetic resonance study

O.C. Alves,^{a,*} E. Wajnberg,^b J.F. de Oliveira,^b and D.M.S. Esquivel^b

^a Dept de Físico-Química, Universidade Federal Fluminense, Niterói, Rio de Janeiro, 14020-150, Brazil

^b Centro Brasileiro de Pesquisas Físicas, Rio de Janeiro, 22290-180, Brazil

Received 18 December 2003; revised 9 March 2004

8 Abstract

9 Temperature dependence of the magnetic resonance is used to study the magnetic material in oriented *Neocapritermes opacus*
10 (N.o.) termite, the only prey of the migratory ant *Pachycondyla marginata* (P.m.). A broad line in the $g = 2$ region, associated to
11 isolated nanoparticles shows that at least 97% of the magnetic material is in the termite's body (abdomen + thorax). From the
12 temperature dependence of the resonant field and from the spectral linewidths, we estimate the existence of magnetic nanoparticles
13 18.5 ± 0.3 nm in diameter and an effective magnetic anisotropy constant, K_{eff} between 2.1 and 3.2×10^4 erg/cm³. A sudden change in
14 the double integrated spectra at about 100 K for N.o. with the long body axis oriented perpendicular to the magnetic field can be
15 attributed to the Verwey transition, and suggests an organized film-like particle system.
16 © 2004 Published by Elsevier Inc.

17 **Keywords:** Magnetic material; Orientation; Termite; Magnetic resonance

18 1. Introduction

19 The *Pachycondyla marginata* (P.m.) ant presents a
20 migratory behavior, relocating the nest sites at irregular
21 time intervals [1]. Most of the migratory process takes
22 place in darkness during the dry/cold season. The mi-
23 gration is significantly oriented at an angle of 13° rela-
24 tive to the magnetic North–South axis [2]. Animal
25 orientation relies on multiple cues, which may some-
26 times interact in complex ways, but the only possible cue
27 to yield this migratory information is the geomagnetic
28 field [3]. This magnetic orientation hypothesis gains in
29 plausibility considering that magnetic iron oxides have
30 been found in this ant [4]. Isolated magnetic nanopar-
31 ticles and aggregates were inferred in the abdomen by
32 magnetic resonance [5] and supported by induced remanent
33 magnetization temperature dependence measure-
34 ments [6].

The P.m. ant is an obligate termite predator that
conducts well-organized predatory raids toward the nests
of its only prey, the *Neocapritermes opacus* (N.o.) termite.
Target termite nests are up to 38 m from the ant colony,
and raids on these nests occur both by day and night, and
can last for more than 24 h [1]. The chemical transfor-
mation of food and nest building by termites have an
important role in nutrition cycles and structural change
of soil in forest and others vegetable ecosystems [7]. N.o.
is usually found in active or inactive nests of other spe-
cies, it lives on vegetables and wood garbage and is
considered one of the most dangerous sugarcane pests.

Due to the termite's ecological aspects, particularly the
prey–predator relation, it became a very attractive species
for magnetic materials studies in social insects. Magnetic
resonance (MR) has proved to be a useful technique for
these studies because of the resonance spectra dependence
on the magnetic structure size and shape. This technique
encompasses enough sensitivity to study inorganic pre-
cursors [8], as well as magnetic materials in ants and bees
[5,9,10]. In this paper, we report on the temperature de-
pendence of the MR spectra of N.o. termites sections,
head and body (thorax + abdomen), to investigate the

* Corresponding author. Fax: +55-21-21417540.

E-mail addresses: cambraia@cbpf.br (O.C. Alves), elianew@cbpf.br, darci@cbpf.br (E. Wajnberg).

58 presence and to compare the properties of the magnetic
59 particles present in these sections.

60 2. Experimental

61 N.o. termites were collected in Campinas, São
62 Paulo, in the Southeast of Brazil, found inside the
63 P.m. nests. Termites were extensively washed with
64 80% (v/v) ethanol and conserved in this solution.
65 Samples were transferred to MR quartz tubes and
66 sealed under nitrogen flux to prevent oxygen contri-
67 butions to the MR signals at low temperatures (below
68 80 K).

69 Samples consist of three heads and one oriented body
70 (abdomen+thorax) of worker termites cooled in a
71 3.4 kOe magnetic field. The orientation effects were
72 studied with the body fixed in MR tubes with vacuum
73 grease, with the magnetic field parallel (z direction),
74 N.o. $_{\parallel}$, and perpendicular (y direction), N.o. $_{\perp}$ to long
75 body axis, as shown in Fig. 1. Heads were not oriented.
76 Four individual bodies were used for repeated temper-
77 ature variation experiments. The results are the average
78 values obtained with three and two experiments for
79 N.o. $_{\perp}$ and N.o. $_{\parallel}$, respectively.

80 Measurements were performed with a commercial X-
81 band ($\nu = 9.442476$ GHz) MR spectrometer (Bruker
82 ESP 300E) operating at a microwave power of 4 mW
83 with a 100 kHz modulation frequency and a modulation
84 field of about 2 Oe in amplitude. A helium flux cryostat
85 (Air products LTD-3-110) was used to control the
86 temperature with an Au-Fe \times chromel thermocouple
87 just below the samples.

88 The absorption derivative resonant field, H_R , and
89 the peak-to-peak linewidth, ΔH , were obtained with
90 the WINEPR software (Bruker), taking H_R at the
91 maximum of the absorption spectra (first integral).
92 Fittings were performed with Origin (Microcal) soft-
93 ware.

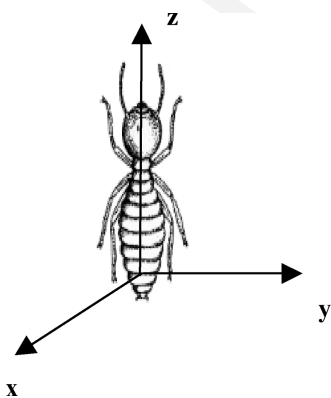


Fig. 1. Termite axis scheme. N.o. $_{\parallel}$, magnetic field parallel to z -axis (the N.o. body long axis), N.o. $_{\perp}$, magnetic field parallel to y -axis direction.

3. Results

95 Fig. 2 shows the N.o. $_{\perp}$ and single head derivative MR
96 spectra at different temperatures. At temperatures
97 higher than 15 ± 4 K both head and N.o. $_{\perp}$ and N.o. $_{\parallel}$
98 (not shown) body spectra consist of a broad
99 ($\Delta H > 1100$ Oe) line at $g \approx 2.0$. The signal intensity de-
100 creases and the linewidth increases as temperature de-
101 creases.

102 At temperatures below 20 K (not shown) the broad
103 line in the head spectra disappears and two narrow lines
104 at $g = 2.066$ and $g = 4.3$ are easily observed (arrows on
105 Fig. 2). Their signal intensity decreases strongly with
106 increasing temperatures and it is not observed at high
107 temperatures. The temperature dependences of N.o. $_{\parallel}$ or
108 N.o. $_{\perp}$ spectra are similar. The spectra broaden asym-
109 metrically and shift to lower magnetic fields when tem-
110 perature decreases. This is the typical high temperature
111 behavior found for different superparamagnetic nano-
112 particles immersed in an inert matrix [11], in glycerol
113 [12], in solid kerosene [13], in sol-gel glass [14,15] and
114 also observed for the MR high field component of P.m.
115 ant abdomen spectra [5].

116 Fig. 3 shows the N.o. $_{\parallel}$, N.o. $_{\perp}$, and N.o. head reso-
117 nance linewidth temperature dependences. The experi-
118 mental data were fitted with the expression (1) for the
119 entire temperature range of the observation

$$H = \Delta H^0 \tan h(\Delta E/2kT), \quad (1)$$

121 where $\Delta H^0 = 5g\beta Sn/d^3$ and $\Delta E = KV$ is mainly associ-
122 ated to the magnetic energy barrier height, K is the
123 magnetic anisotropy constant and V is the particle vol-
124 ume. The ΔH^0 prefactor, which is the ΔH low temper-
125 ature limit, includes the Bohr magneton, β , the spin
126 associated to the magnetic nanoparticle center, S , the

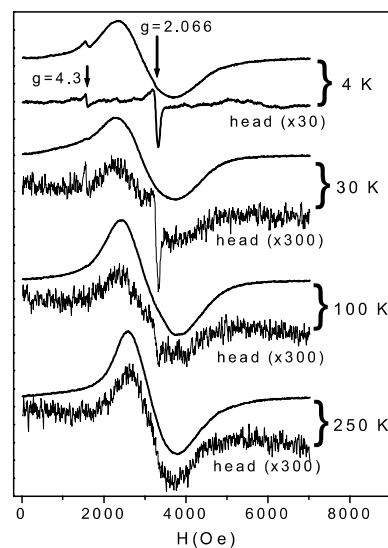


Fig. 2. Temperature dependence of N.o. $_{\perp}$ and a single head magnetic resonance spectra.

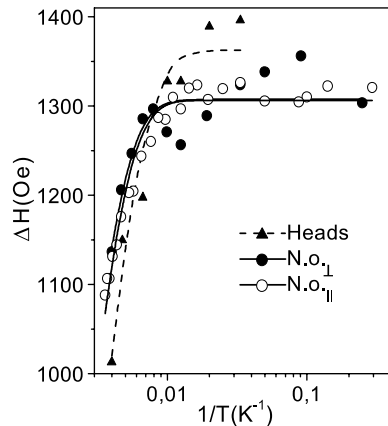


Fig. 3. Spectra linewidth temperature dependence. The solid and dashed lines are the best fits of Eq. (1) for the body (N.o._∥ and N.o._⊥) and head data, respectively, with the parameters given in Table 1.

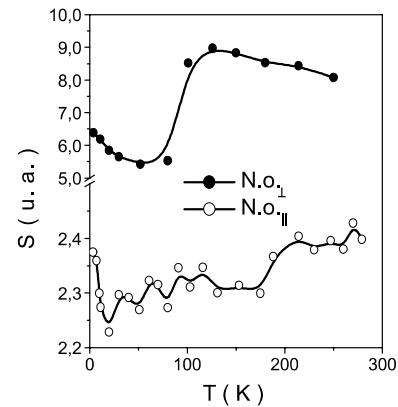


Fig. 5. Temperature dependence of MR spectra absorption area, $S = I_{pp}\Delta H^2$, showing that at 250 K the N.o._⊥ value is almost three times that of N.o._∥.

127 number of magnetic centers in the particle, n , and the
128 particle-particle distance, d . The best-fit parameters are
129 listed in Table 1 and, for comparison, the P.m. abdomen
130 values are also given.

131 Fig. 3 and the data in Table 1 show that the N.o._∥ and
132 N.o._⊥ linewidth data present, within the experimental
133 error, the same behavior with $KV = (9.1 \pm 0.5) \times 10^{-21}$ J,
134 while for N.o. head $KV = (6.7 \pm 0.4) \times 10^{-21}$ J. The same
135 is observed for the limiting low temperature value (the

Table 1
N.o. termite and P.m. migratory ant fitting parameters of Eq. (1)

	H_R^0 (Oe)	$\Delta E/2k$ (K ⁻¹)	Temperature fitting range
N.o. _∥	1306 ± 4	320 ± 4	4–279 K
N.o. _⊥	1307 ± 10	336 ± 20	4–279 K
N.o. head	1363 ± 19	242 ± 13	>20 K
P.m. abdomens ^a	1373 ± 10	272 ± 7	>70 K

^a From [5].

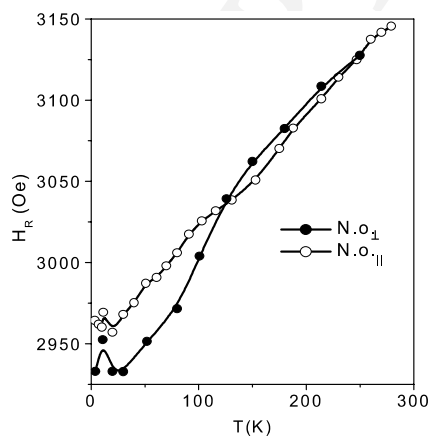


Fig. 4. Temperature dependence of resonant field, H_R . Solid lines are guide to the eyes.

prefactor ΔH^0) which is distinguishable only for the
136 head part. 137

The N.o._∥ and N.o._⊥ resonant magnetic field (H_R)
138 temperature dependences are similar (Fig. 4). A smooth
139 inflection is more easily observed in the 100 K region for
140 the perpendicular orientation. The head data also present
141 a shift in this temperature range, but it is within the
142 error bars much larger than those of the body data,
143 because of the $g = 2.066$ superimposed line (not shown). 144

The peak-to-peak amplitude, I_{pp} (not shown) and the
145 double integration of the MR (area under absorption
146 curve) S are proportional to the magnetic particle
147 number. At 250 K the second integration of the N.o._⊥
148 body line is 250 times larger than that of a single head
149 while this value decreases to 70 for the N.o._∥ line. The
150 magnetic material is predominantly in the N.o. body
151 (about 99 and 97% considering the N.o._⊥ and N.o._∥
152 body orientation, respectively). The N.o._⊥ area values
153 are almost three times those of the N.o._∥, showing a
154 lower number of magnetic particles in the specimens
155 used for the parallel orientation (Fig. 5). Variability of
156 the amount of magnetic material in insects has already
157 been observed in bees and termites [16,17]. 158

The S temperature dependence is sensitive to the N.o.
159 body orientation relative to the magnetic field. The
160 N.o._⊥ presents a sudden increase at nearly 90 ± 10 K,
161 not observed for N.o._∥, strengthening the behavior ob-
162 served for the ΔH (Fig. 3) and H_R (Fig. 4) temperature
163 dependences. 164

4. Discussion

At low temperatures the MR spectra of heads pre-
166 sents only two lines at $g = 4.3$ and $g = 2.066$. The first
167 one was observed in other social insects [5,9,10] and was
168 associated to magnetically isolated high spin ($S = 5/2$)
169 Fe^{3+} ions in a low symmetry environment [18]. Its signal
170

165

166
167
168
169
170

intensity decreases strongly with increasing temperatures and it is not observed at high temperatures. A line similar to the $g = 2.066$ one was observed in horse spleen ferritin solution [19] and when ferritin core is developed from Fe^{2+} and O_2 in apoferritin. It was suggested that it involves a hydroxyl radical formation as a by-product of the core formation, once that iron under aerobic conditions is capable of producing these radicals [20]. It was neither observed in the N.o. body nor in P.m. and honeybee abdomens, either because of the much higher intensity of the broad line in these samples or because it is not formed.

The broad line could not be followed to temperatures lower than 20 K, suggested as the Neel temperature of uncompensated spins in horse spleen ferritin [19]. Ferritin was found in the endoplasmatic reticulum and secretory pathway of nine families from six insect orders [21]. Electron microscopy analysis suggest that microcrystals containing iron found in leafhoppers gut are comprised of ferritin with 6 nm core diameters [22], similar to those reported for mammalian ferritin.

Considering the system as composed by spherical nanoparticles, with no demagnetization field contribution, the resonant field is given by $H_R(T) = \omega_R / \gamma - H_A(T)$, where ω_R is the resonance frequency, γ is the gyromagnetic ratio and H_A the effective anisotropy field. Using the experimental values of ω_R and $\gamma = 1.87 \times 10^7 \text{ Oe}^{-1} \text{ s}^{-1}$ ($g = 2.13$) extrapolated at the high temperature limit ($H_R = 3166 \text{ Oe}$) at which the H_A is expected to be null, the temperature dependence of H_A is obtained (Fig. 6). For spherical nanoparticles H_A is given by $2K_{\text{eff}}/M_S$, where K_{eff} is the effective magnetocrystalline anisotropy density and M_S is the saturation magnetization, characteristic of the magnetic material.

Under the hypothesis of ferritin particles, taking the horse spleen ferritin magnetic moment as $345\mu_B$ [23] and

$200\mu_B$ [24], M_S ferritin values are estimated as 16.4 and 28.3 Oe, respectively. From H_A values averaged in the experiment temperature range (Fig. 6), $K = 7.3 \times 10^2$ and $12 \times 10^2 \text{ erg/cm}^3$ are calculated, which together with ΔE values from Table 1 yield a diameter larger than 47 nm, which falls outside the insect ferritin ranges. Although the ferritin contribution cannot be completely discarded, the MR spectra may indicate that it is a magnetite core formation in ferritin, as observed in human brain tissues [25] or a ferritin–magnetite transformation. The highly toxic Fe^{2+} is taken by the protein and oxidized, to be stored as less toxic Fe^{3+} , in the form of ferrihydrite [26]. If the ferritin core becomes overloaded or there is a breakdown in the protein's function, a mechanism for Fe^{2+} oxidation is lost, leading to the formation of biogenic magnetite that contains alternating lattice of Fe^{2+} and Fe^{3+} [27].

On the other hand, magnetite is the most common biomineralized material, with $g = 2.12$ [28,29] in good agreement with the limit value calculated above, and M_S as 470 Oe. From the H_A values, K_{eff} values are then obtained as $(2.6 \pm 0.1) \times 10^4$, $(3.2 \pm 0.2) \times 10^4$, and $(2.1 \pm 0.1) \times 10^4 \text{ erg/cm}^3$ for N.o. $_{\parallel}$, N.o. $_{\perp}$, and N.o. head, respectively. Using these values and the $\Delta E = KV$ values given in Table 1, the same average magnetic volumes of $(3.2 \pm 0.3) \times 10^3 \text{ nm}^3$ are obtained for body and head particles, and correspond to a diameter of $18.5 \pm 0.3 \text{ nm}$. As n is proportional to the particle volume, the prefactors in Table 1 indicate shorter particle–particle distances in the head than in the body.

At low temperatures bulk magnetite undergoes a phase transition already observed by anomalies in electrical and magnetic properties, such as an abrupt changes in K [28] or in the magnetic susceptibility [30]. The intensity and temperature of this transition depend on the stoichiometry [29], impurities or derivative substitutes [31,32] and molar ratio of Fe^{3+} and Fe^{2+} [33]. Nevertheless magnetic properties behavior of layers can differ considerably from bulk behavior as a result of substrate induced strain or relatively large contribution of an altered anisotropy at the interface, associated to different growth technique and/or substrate material [34–36].

A sharp transition was observed in the temperature dependence of the perpendicular resonant field of ultrathin Fe_3O_4 layers grown on different substrate films [34,36]. Its intensity and shape was shown to depend on the thickness of magnetic film. It takes place at about 105 K, for magnetic layer thickness from 5 to 200 nm [36] and is hardly detectable for thickness below 5 nm [34]. This transition was associated to the magnetite Verwey temperature.

The area under the absorption curve, S , was shown to correlate to the magnetic susceptibility in ferrihydrite nanoparticles [37]. The S transition observed is associated to the susceptibility bulk transition cited above,

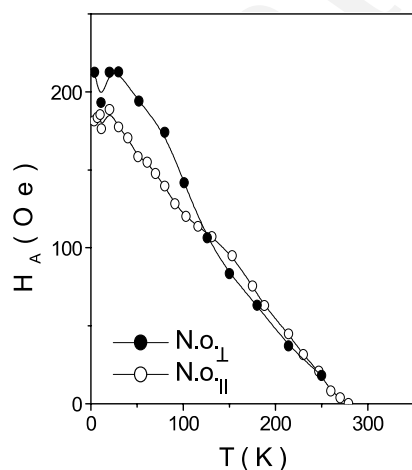


Fig. 6. Temperature dependence of anisotropy field, H_A , calculated from the resonant field curves in Fig. 4.

264 with a modified shape as in a layer structure and the
265 temperature dependence of ΔH and H_R for N.o. $_{\perp}$ sug-
266 gest the film-like configuration perpendicular to the
267 resonant field.

268 5. Conclusions

269 This paper presents a novel application of MR to
270 determine the organization and magnetic parameters of
271 iron oxide particles in termites. MR data show that 97–
272 99% of the magnetic material is in the N.o. termite body.
273 Magnetization measurements indicate a less asymmetric
274 distribution in another termite species, *Nasutitermes*
275 *exitiosus*, with about 77% of the material in the body [17],
276 while 34% of the saturation magnetization comes from
277 the P.m. ant body contribution (in press, Biometals).

278 The nanoparticles in the head could only be derived
279 from biomineralization and/or cuticular contamination
280 processes [4] while in the body they could be due to
281 biomineralization and the accumulation of ingested
282 materials in the digestive apparatus. Although the latter
283 case cannot be related to a magnetic orientation process,
284 the magnetic anisotropy changes observed and the sug-
285 gested geometric arrangement indicate that some of the
286 nanoparticles in N.o. body are involved with the mag-
287 netoreception process. Although there is no report on
288 magnetoreception for N.o., it was observed in foraging
289 of another termite species, *Trinervitermes geminatus* [38].

290 Since MR spectra of N.o. oriented parallel (N.o. $_{\parallel}$) or
291 perpendicular (N.o. $_{\perp}$) to the magnetic field ought to be
292 due to the same particle system, the differences between
293 the parallel and perpendicular orientation behaviors can
294 be related to the magnetic particles arrangement. A
295 particle system in the zx body plane with the easy
296 magnetization axis close to the y direction, perpendic-
297 ular to the N.o. body axis (Fig. 1) could account for this
298 result. Similarly, magnetite nanoparticles aligned trans-
299 versely to the body axis on the horizontal plane were
300 observed in the honeybee [16]. This effect was not ob-
301 served in MR studies of honeybee abdomens [9] because
302 crushing of the sample disrupted the particles arrange-
303 ment. The present study with an intact oriented sample
304 allowed us to verify the structural organization of the
305 particles in the body of the termite.

306 A much larger quantity of isolated nanoparticles was
307 found in N.o. termite specie as compared to its predator,
308 the P.m. ant, with similar remanent to saturation mag-
309 netization ratio, J_R/J_S , within the magnetite pseudo
310 single domain (PSD) or multi domain (MD) region (in
311 press, JMMM). These P.m. ant abdomens MR spectra
312 at high temperatures were characterized by two broad
313 main components: the high field ($g \sim 2$) related to iso-
314 lated magnetic nanoparticles and the low field (g in the
315 range from 5 to 6.3) related to aggregate or large par-
316 ticles [5]. Clusters or larger particles are not observed in

N.o. termites, as the low field line is not present in their
spectra.

The different magnetic diameters estimated for iso-
lated particles, 18.5 ± 0.3 nm for termites and
 13 ± 0.4 nm for ants [5], as well as reported different H_C
values (in press, JMMM) suggest that the ant predator
does not make direct use of the termite prey magnetic
material, no matter whether ingested or biomineralized.
Nanoparticle magnetic properties are sensitive to the
size, shape, organization, and particle–particle distance.
If these particle systems are related to the sensorial
system these differences could account for their specific
magnetoreception mechanism. While in microorganisms
the size and appearance of magnetite biomineralized
crystals are specie-specific and uniform within a single
cell with a narrow size distribution [39,40], in animals
this kind of study is just beginning. In the this context,
the differences observed in MR spectra of N.o. termites
and P.m. ants, related to the differences in biomineral-
ization and accumulation process of magnetite, should
be associated to their role in the predator–prey rela-
tionship. This subject opens a branch of study for the
biomineralization process under the ecological and
evolutionary point of view.

Acknowledgments

We thank Dr. P.S. Oliveira for termite supply, Dr. G.
Bemski for the comments and Dr. D. Ellis for carefully
reading the manuscript. E.W. and D.M.S.E. thank
CNPq and FAPERJ for financial support and J.F.O.
thanks the CNPq for a fellowship.

References

- [1] I. Leal, P.S. Oliveira, Behavioral ecology of the neotropical
termite-hunting ant *Pachycondyla* (= *Termitopone*) *marginata*:
colony founding, group-raiding and migratory patterns, *Behav.*
Ecol. Sociobiol. 37 (1995) 373–383.
- [2] D. Acosta-Avalos, D.M.S. Esquivel, E. Wajnberg, H.G.P. Lins de
Barros, P.S. Oliveira, I. Leal, Seasonal patterns in the orientation
system of the migratory ant *Pachycondyla marginata*, *Naturwis-*
senchaften 88 (2001) 343–346.
- [3] R. Wiltschko, W. Wiltschko, *Magnetic Orientation in Animals*,
Springer, Berlin, 1995.
- [4] D. Acosta-Avalos, E. Wajnberg, P.S. Oliveira, I. Leal, M. Farina,
D.M.S. Esquivel, Isolation of magnetic nanoparticles from
Pachycondyla marginata ants, *J. Exp. Biol.* 202 (1999) 2687–2692.
- [5] E. Wajnberg, D. Acosta-Avalos, L.J. El-Jaick, L. Abraçado, J.L.
Coelho, A.F. Bakuzis, P.C. Morais, D.M.S. Esquivel, EPR study
of migratory ant *Pachycondyla marginata* abdomens, *Biophys. J.*
78 (2000) 1018–1023.
- [6] E. Wajnberg, G. Cernicchiaro, D. Acosta-Avalos, L.J. El-Jaick,
D.M.S. Esquivel, Induced remanent magnetization of social
insects, *J. Magn. Magn. Mater.* 2040 (2001) 226–230.
- [7] E.R. Laffont, Available from <<http://www.unne.edu.ar/cyt/2001/6-Biologicas/B-044.pdf>>.

- 370 [8] R. Berger, J. Kliava, J.C. Bissey, V. Baietto, Superparamagnetic
371 resonance of annealed iron-containing borate glass, *J. Phys.*
372 *Condens. Matter* 10 (1998) 8559–8572.
- 373 [9] L.J. El-Jaick, D. Acosta-Avalos, D.M.S. Esquivel, E. Wajnberg,
374 M.P. Linhares, EPR study of Honeybees *Apis mellifera* abdomens,
375 *Eur. Biophys. J.* 29 (2001) 579–586.
- 376 [10] D.M.S. Esquivel, D. Acosta-Avalos, L.J. El-Jaick, A.D.M.
377 Cunha, M.G. Malheiros, E. Wajnberg, M.P. Linhares, Evidence
378 for magnetic material in the fire ant *Solenopsis* sp by electron
379 paramagnetic resonance measurements, *Naturwissenschaften* 86
380 (1999) 30–32.
- 381 [11] P.C. Morais, M.C.F. Lara, K. Skeff Neto, Electron spin resonance
382 in superparamagnetic particles dispersed in a non-magnetic
383 matrix, *Philos. Mag.* 55 (1987) 181–183.
- 384 [12] F. Gazeau, V. Shilov, J.C. Bacri, E. Dubois, F. Gendron, R.
385 Perzynski, Y.L. Raikher, V.I. Stepanov, Magnetic resonance of
386 nanoparticles in a ferrofluid: evidence of thermofluctuational
387 effects, *J. Magn. Magn. Mater.* 202 (1999) 535–546.
- 388 [13] K. Nagata, A. Ishihara, ESR of ultrafine magnetic particles, *J.*
389 *Magn. Magn. Mater.* 104 (1992) 1571–1573.
- 390 [14] R. Berger, J.C. Bissey, J. Kliava, H. Daubric, C. Estournes,
391 Temperature dependence of superparamagnetic resonance of iron
392 oxide nanoparticles, *J. Magn. Magn. Mater.* 234 (2001) 535–544.
- 393 [15] C.T. Hsieh, W.L. Huang, J.T. Lue, The change from paramagnetic
394 resonance to ferromagnetic resonance for iron nanoparticles made
395 by the sol–gel method, *J. Phys. Chem. Sol.* 63 (2002) 733–741.
- 396 [16] J.L. Gould, J.L. Kirschvink, K.S. Deffeyes, Bees have magnetic
397 remanence, *Science* 201 (1978) 1026–1028.
- 398 [17] B.A. Maher, Magnetite biomineralization in termites, *Proc. Roy.*
399 *Soc. Lon. B* 265 (1998) 733–737.
- 400 [18] E.M. Yahiaoui, R. Berger, Y. Servant, J. Kliava, L. Cugunov, A.
401 Mednis, Electron-paramagnetic-resonance of Fe³⁺ ions in borate
402 glass–computer-simulations, *J. Phys. Condens. Matter* 6 (1994)
403 9415–9428.
- 404 [19] E. Wajnberg, L.J. El-Jaick, M.P. Linhares, D.M.S. Esquivel,
405 Ferromagnetic resonance of horse spleen ferritin: core blocking
406 and surface ordering temperatures, *J. Magn. Reson.* 153 (2001)
407 69–74.
- 408 [20] J.K. Grady, Y. Chen, N.D. Chasteen, D.C. Harris, Hydroxyl
409 radical production during oxidative deposition of iron in ferritin,
410 *J. Biol. Chem.* 264 (1989) 20224–20229.
- 411 [21] H. Nichol, M. Locke, The localization of ferritin in insects, *Tissue*
412 *cell* 22 (1990) 767–777.
- 413 [22] M. Kimura, L. Seveus, K. Maramorosch, Ferritin in insect vectors
414 of maize streak disease agent—electron-microscopy and electron-
415 microprobe analysis, *J. Ultra. Mol. Struct. Res.* 53 (1975) 366–
416 373.
- 417 [23] S.A. Makhlof, F.T. Parker, A.E. Berkowitz, Magnetic hysteresis
418 anomalies in ferritin, *Phys. Rev. B* 55 (1997) R14717–14720.
- 419 [24] M.E.Y. Mohie-Eldin, R.B. Frankel, L. Gunther, A comparison of
420 the magnetic-properties of polysaccharide iron complex (pic) and
421 ferritin, *J. Magn. Magn. Mater.* 135 (1994) 65–81.
- [25] C. Quintana, M. Lacin, C. Marhic, M. Perez, J. Avila, J.L. Carrasco, Initial studies with high resolution TEM and electron energy loss spectroscopy studies of ferritin cores extracted from brains of patients with progressive supranuclear palsy and Alzheimer disease, *Cell. Mol. Biol.* 46 (2000) 807–820.
- [26] P.M. Harrison, P. Arosio, Ferritins: molecular properties, iron storage function and cellular regulation, *Biochim. Biophys. Acta* 1275 (1996) 161–203.
- [27] J. Dobson, Nanoscale biogenic iron oxides and neurodegenerative disease, *FEBS Lett.* 496 (2001) 1–5.
- [28] K. Abe, Y. Miyamoto, S. Chikazumi, Magnetocrystalline anisotropy of low-temperature phase of magnetite, *J. Phys. Soc. Jpn.* 41 (1976) 1894–1902.
- [29] Z. Kakol, J.M. Honig, Influence of deviations from ideal stoichiometry on anisotropy parameters of magnetite Fe_{3(1-δ)}O₄, *Phys. Rev. B* 40 (1989) 9090–9097.
- [30] K.P. Belov, Electronic processes in magnetite (magnetite mysteries), *Phys. Uspekhi* 36 (1993) 380–391.
- [31] V.A.M. Brabers, F. Walz, H. Kronmuller, Impurity effects upon the Verwey transition in magnetite, *Phys. Rev. B* 58 (1998) 163–166.
- [32] Y.A. Koksharov, D.A. Pankratov, S.P. Gubin, I.D. Kosobudsky, M. Beltran, Y. Khodorkovsky, A.M. Tishin, Electron paramagnetic resonance of ferrite nanoparticles, *J. Appl. Phys.* 89 (2001) 2293–2298.
- [33] M. Hagiwara, K. Nagata, K. Nagata, Magnetism and magnetic interaction in a complex oxide glass system containing deposited clusters of magnetite at the superparamagnetic state, *J. Phys. Soc. Jpn.* 67 (1998) 3590–3600.
- [34] P.A.A. van der Heijden, M.G. van Opstal, C.H.W. Swüste, P.H.J. Bloemen, J.M. Gaines, W.J.M. Jonge, A ferromagnetic resonance study on ultra-thin Fe₃O₄ layers grown on (001)MgO, *J. Magn. Magn. Mater.* 182 (1998) 71–80.
- [35] J. Tang, K. Wang, W. Zhou, Magnetic properties of nanocrystalline Fe₃O₄ films, *J. Appl. Phys.* 89 (2001) 7690–7692.
- [36] S. Kale, S.M. Bhagat, S.E. Lofland, T. Scabarozzi, S.B. Ogale, A. Orozco, S.R. Rhinde, T. Venkatesan, B. Hannoyer, B. Mercey, W. Prellier, Film thickness and temperature dependence of the magnetic properties of pulsed-laser-deposited Fe₃O₄ films on different substrates, *Phys. Rev. B* 64 (2001) 205413.
- [37] M.S. Seehra, A. Punnoose, A. Manivannan, Effect on Si doping on the electron spin resonance properties of ferrihydrite nanoparticles, *IEEE Trans. Magn.* 37 (2001) 2207–2209.
- [38] M. Rickli, R.H. Leuthold, Homing in harvester termites—evidence of magnetic orientation, *Ethology* 77 (1988) 209–216.
- [39] D. Schuler, Molecular analysis of a subcellular compartment: the magnetosome membrane in *Magnetospirillum gryphiswaldense*, *Arch. Microbiol.* 181 (2004) 1–7.
- [40] D.M.S. Esquivel, H.G.P. Linsde Barros, M. Farina, Diversity of magnetic crystals found in magnetotactic bacteria, in: R.B. Frankel, R.P. Blakemore (Eds.), *Iron Biominerals*, Plenum Press, New York, 1991.